Electronic Supplementary Information for

Unveiling new stable Manganese based photoanode materials via theoretical high-throughput screening and experiments

Juhwan Noh,[†,#] Sungwon Kim,[†] Geun ho Gu,[†] Aniketa Shinde,[‡,#] Lan Zhou,[‡] John M. Gregoire,[*,‡] and Yousung Jung[*,†]

[†] Department of Chemical and Biomolecular Engineering, Korea Advanced Institute of Science and Technology (KAIST)291 Daehak-ro, Yuseong-gu, Daejeon 34141, Republic of Korea

[‡] Joint Center for Artificial Photosynthesis, California Institute of Technology, Pasadena, CA 91125, USA

[#] These authors contributed equally to this work.

*Correspondence: gregoire@caltech.edu, ysjn@kaist.ac.kr

S1. Methodology

S1.1 Computational detail

For dataset construction, we performed spin-polarized PBE+U [1, 2]calculations and PAW[3]-PBE pseudopotentials as implemented in the *ab initio* package, VASP,[4] and we used 3.9 as U-value for Mn taken from Materials Project.[5] We relaxed both atomic positions and unit cell parameters using conjugate gradient descent method with convergence criteria of 1.0e-5 for energy and 0.05 $eV/\text{Å}$ for force with 500 eV cut-off energy. To consider computational efficiency, Brillouin zone is used with k-point densities at or larger than 500 k-points per atoms using the *Pymatgen* package.[6] Duplicates for the converged structures are removed using the *StructureMatcher* function implemented in *Pymatgen* package.[6] After passing tier 1, we performed the latter computations with dense k-space (i.e. Brillouin zone with k-point densities at or larger than 1000 k-points per atoms using the *Pymatgen* package[6]). To compute the energy above the convex hull, we followed GGA/GGA+U mixed approach proposed by A. Jain et al[7]. In the latter approach, the energy of all GGA+U[1, 2] calculations is corrected by equation S1.

$$E^{GGA+U\ renorm.}_{Mn,O\ compound} = E^{GGA+U}_{Mn,O\ compound} - n_{Mn}\Delta E_{Mn} \qquad \text{(S1)}$$

In equation (S1), $E^{GGA+U\ renorm.}_{Mn,O\ compound}$ is the GGA+U energy for Mn, O compound and n_{Mn} is the number of Mn atoms in the compound. Here, our target is to obtain a correction term ΔE_{Mn} for Mn. In addition, we included an O_2 energy correction term (equation S2) taken from the MP database for the $E^{GGA+U}_{Mn,O\ compound}$ energy.

$$E(O_2)_{corr.} = -1.4046eV/O_2 \qquad \text{(S2)}$$

After a simple rearrangement using equation (S1), the correction energy for V atom is then obtained using equation (S3).

$$\Delta E_{Mn} = (E^{ref.}_f - Calc.E_f)/r_{Mn} \qquad \text{(S3)}$$

In equation (S3), $E^{ref.}_f$ is the formation energy for the 4-reference structures (MnO, MnO_2, Mn_2O_3 and Mn_3O_4) taken from the MP database all of which are at the ground state for the corresponding composition, $Calc.E_f$ is the formation energy calculated from this work, and r_{Mn} is the fraction of Mn atom in a compound. Therefore, ΔE_{Mn} can be interpreted as the slope of the $(E^{ref.}_f - Calc.E_f)$ vs. r_{Mn} plot as shown in Fig. S1a. The value of ΔE_{Mn} for each case is shown in Fig. S1a, and the adjusted formation energy values are described in Fig. S1b.

(a)

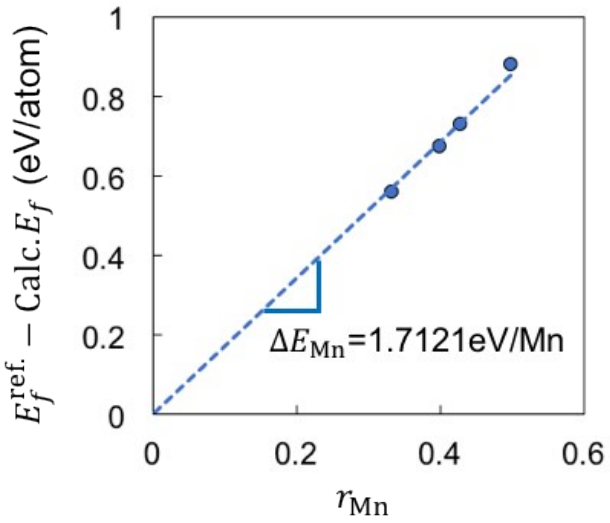

(b)

	Materials		Ef from MP	After correction
mp-18759	Mn_3O_4	$I4_1/amd$	-2.063	-2.069
mp-19006	MnO	Fm-3m	-2.000	-1.977
mp-565203	Mn_2O_3	Pbca	-2.028	-2.040
mvc-12022	MnO_2	I4/m	-1.811	-1.824

Fig. S1 (a) Deriving correction energy for Mn ($^{\Delta E_{Mn}}$) using the GGA/GGA+U-mixed scheme for the 4-Mn_xO_y materials at the convex hull, and (b) results after applying the latter correction energy terms for the 4-Mn_xO_y materials at the convex hull (in eV/atom).

S1.2 Band gap calculations

We performed HSE[8] hybrid DFT functional implemented in VASP[4] with a mixing parameter of 0.2. For computational efficiency, a uniform reduction factor for the q-point grid of the exact exchange potential is applied (NKRED = 2) with gamma centered even number k-points (with a k-point densities at or larger than 1000 k-points per atoms).

S1.3 Band-level alignment with respect to vacuum

The band alignment of water redox potential for the Mg_2MnO_4-a with respect to vacuum were calculated with the surface PBE+U[1, 2] slab computations assuming ferromagnetic ordering of initial spin state for simplicity. All the surface slabs are constructed from the workflow implemented in the *Pymatgen*,[6,9] and 1.5nm vacuum is applied. Following the previous work,[10, 11] we only consider low Miller index (^{h,k,l}) where the maximum value is 1, and non-polar surfaces since those surfaces are typically lowest energy. The surface energy of the computed slabs are defined as $E_{surf} = \frac{E_{slab} - E_{bulk}}{2A}$ where E_{slab} is the total energy of slab, E_{bulk} is the total energy of bulk with same number of atoms, and A is the surface area. In main text, we only reported the results of most stable surface configuration, <110>.

S1.4 Experimental details

The synthesis proceeded in a custom combinatorial sputter deposition system[12] (Kurt J. Lesker PVD75) with Mg and Mn sources (elemental metal targets) operated at 110 W and 120 W, respectively, in an atmosphere of 0.016 Pa O_2 and 0.784 Pa Ar. The annealing proceeded in a box oven (Thermo, Lindberg Blue M) with flowing air. X-ray diffraction patterns were measured at beamline 1-5 at the Stanford Synchrotron Radiation Laboratory using a combinatorial diffraction instrument described previously.[13] A monochromated 13 keV source with a 1 mm^2 footprint was used with a Princeton Quad-RO 4320 detector in reflection scattering geometry. Diffraction images were processed into XRD patterns using WxDiff software.[14] XRF measurements were performed on an EDAX Orbis Micro-XRF system and analyzed via comparison with thin film standards for both Mg and Mn, with data processing performed in the thin film limit without considering matrix effects. Photoelectrochemistry was performed using a high throughput scanning drop cell[15] with toggled illumination from a 385 nm light emitting diode (ThorLabs M385F1, 820 mW cm^{-2}) and additional details described previously[16].

S1.5 XRD and PEC analysis details

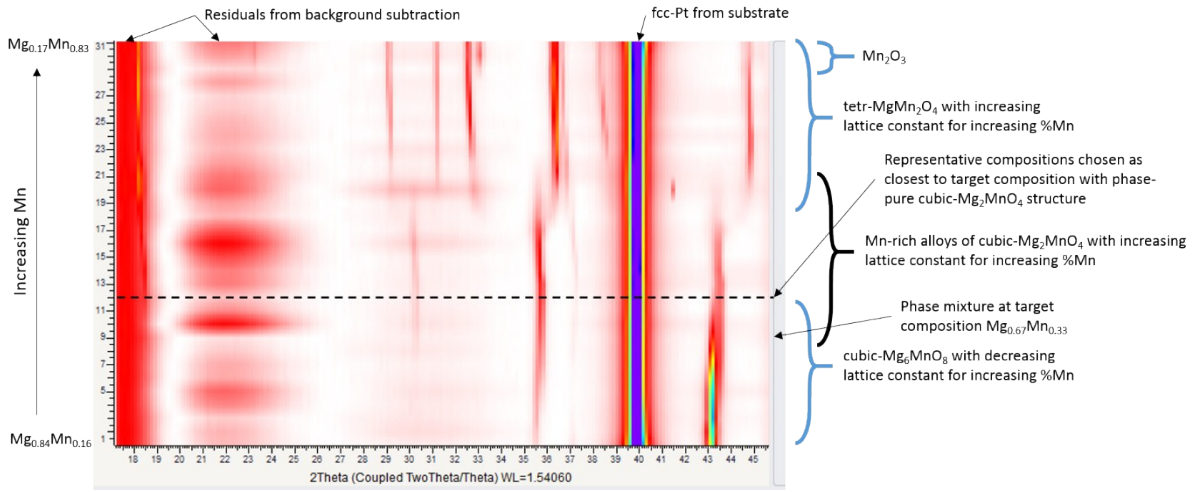

Fig. S2 2D XRD heatmap showing a series of 31 XRD patterns (3 mm grid) along the composition gradient of the Mg-Mn oxide library annealed at 850 °C with Mn concentration from 0.16 to 0.83.

XRD characterization of the as-synthesized Mg-Mn oxide library is summarized in Fig. S2 and reveals the presence of a phase-pure cubic Mg_2MnO_4–a structure at Mn-rich compositions range from 0.48 to 0.62, and an increasing of lattice constant as more Mn alloying in cubic Mg_2MnO_4 structure. It also reveals a phase mixture with the cubic Mg_6MnO_8 structure at Mn concentration below 0.48 and a phase transformation to tetragonal $MgMn_2O_4$ structure at Mn concentration beyond 0.62. Phase pure Mg_6MnO_8 is observed at Mg-rich compositions and is also found to be photoactive, although those results are not pertinent to the present prediction and validation of Mg_2MnO_4–a as a photoanode. Since a phase mixture with this phase is observed at the target composition, the phase(s) responsible for the photoactivity at this composition cannot be determined. While using a Mn-rich alloy of the predicted compound is not ideal for validating the prediciton, the synthesis of thin films suitable for PEC

characterization yield this alloy phase behavior and necessitate the use of the Mn-rich composition to ensure photoactivity from the structure of interest.

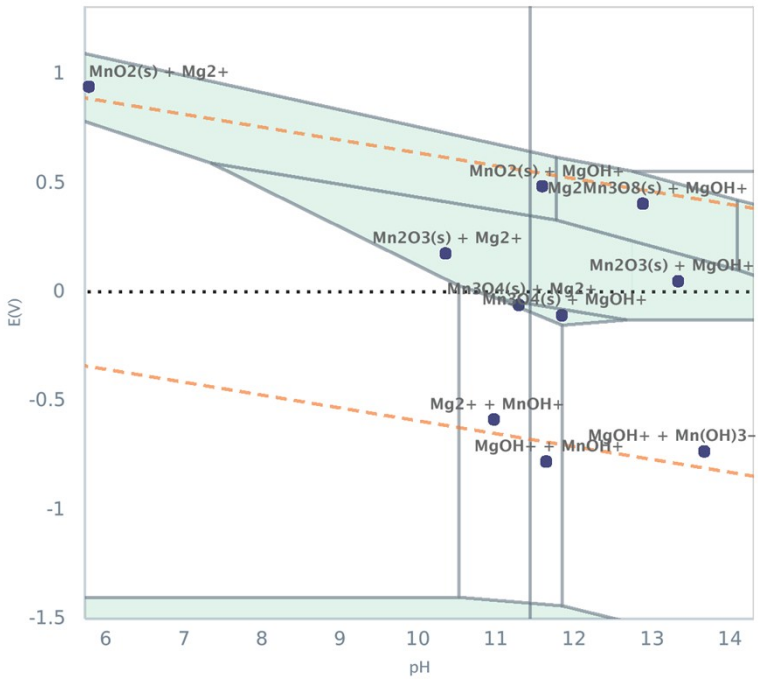

Fig. S3 Pourbaix diagram generated form the Materials Project for the composition $Mg_{0.5}Mn_{0.5}$ with 1.E-8 M of metal species for both elements.[16] Near OER potential at pH 10, the thermodynamically stable phases are MnO_2 (solid) and Mg^{+2} (aq).

XRF analysis was performed on the sample from Fig. 4 before and after (photo)electrochemistry as well as a duplicate sample before and after exposure to the same electrolyte for the same duration but held under open circuit. For both of these films, 0.75 ± 0.05 nmol mm^{-2} of Mg dissolved into electrolyte. At pH 10, Pourbaix analysis indicates that Mg may dissolve as Mg^{+2} over a large potential range, which is consistent with the chemical dissolution of Mg and corresponds to electrochemical or photoelectrochemical dissolution of Mg. The extent of Mg corrosion is consistent with the formation of a 13 nm-thick passivation layer of MnO_2, which is similar to the dissolution of V and formation of CuO passivayion layer in copper vanadate photoanodes.[17] This passivation layer may also serve as a cocatalyst during photoanode operation. While negligible Mn loss of 0.02 ± 0.05 nmol mm^{-2} was observed in the chemical exposure to electrolyte, 0.12 ± 0.05 nmol mm^{-2} of Mn loss was observed after the PEC expeirment of Fig. 4, indicating some (photo)electrochemical corrosion that is likely due to the CV scanning of potential up to 1.73 V vs RHE. Study of potential-dependent corrosion and passivation will be required for further development of this photoanode, and for the present purposes we note that this Mn dissolution is more than 10 times smaller than the net anodic charge (1.4 nmol mm^{-2} of e^-), indicating that the photoanodic current has no substantial contribution from photocorrosion.

S2. Dataset construction

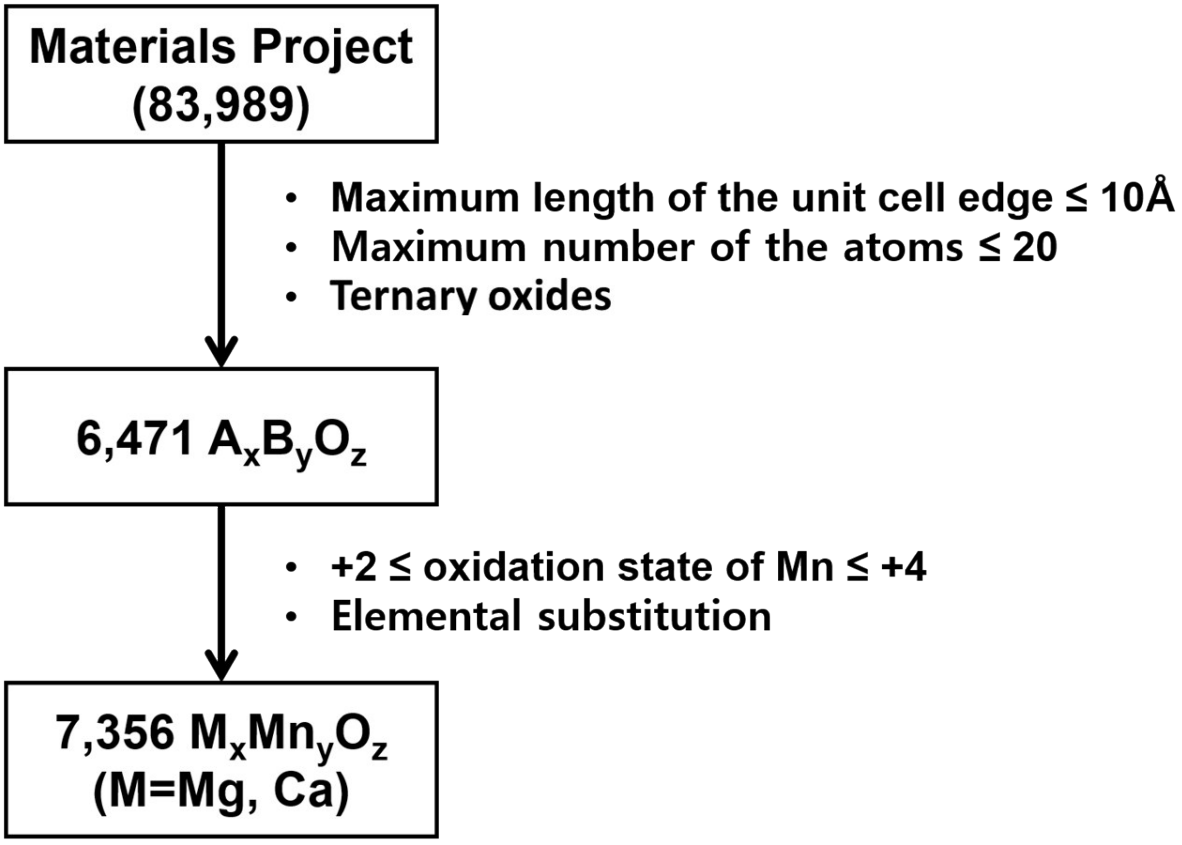

Fig. S4 Processes for dataset construction used in this work. For the first step, we take all ternary oxide materials satisfying the listed constraints (i.e. materials with small unit cell) yielding total 6,471 $A_xB_yO_z$ materials. For the latter, we applied elemental substitution as mentioned in the main text yielding 7,356 $Mg_xMn_yO_z$ and 7,356 $Ca_xMn_yO_z$ materials.

S3. Computed E^* for [Mg,Ca]-Mn-O at tier 1

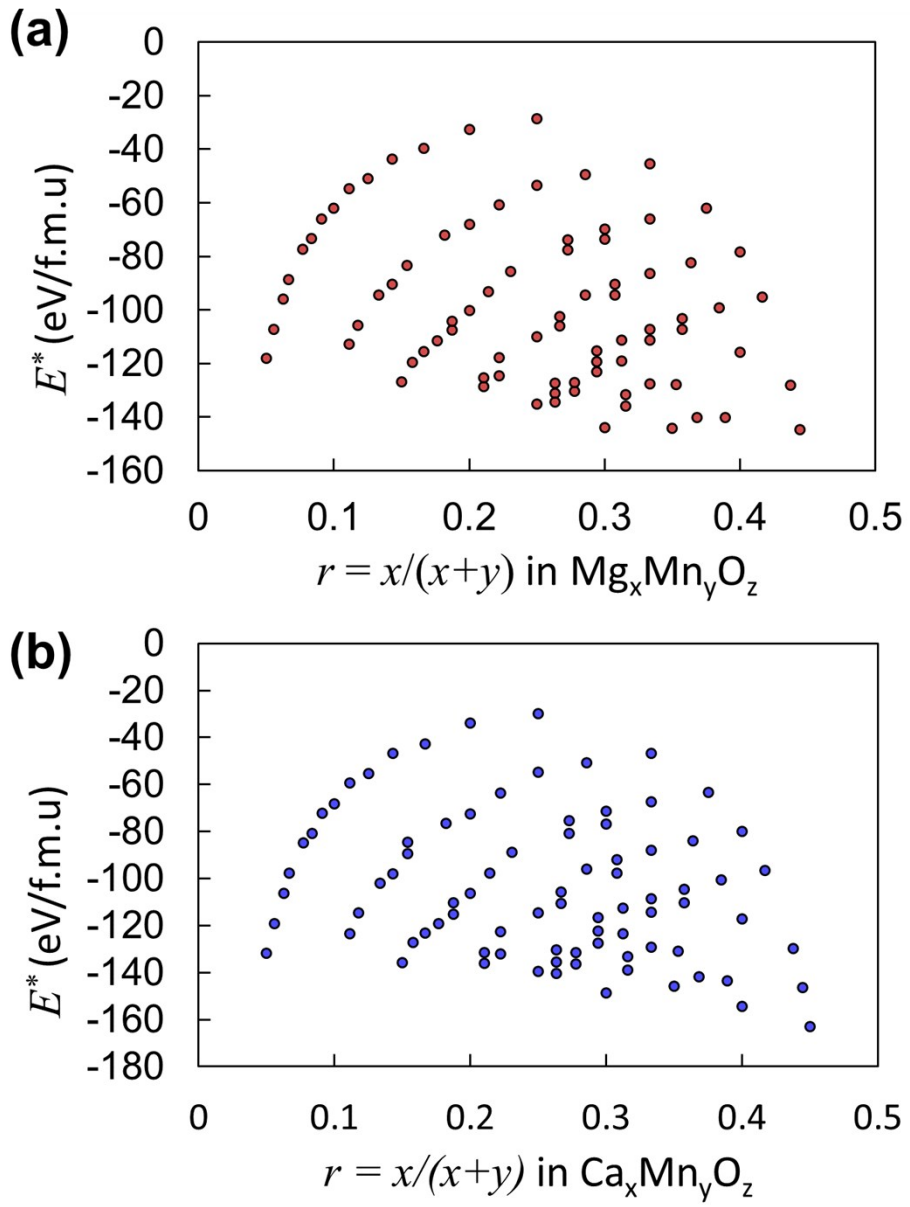

Fig. S5 Computed the upper bound of energy (E^*) satisfying $\Delta G_{pbx}^{min} = 0.80$ eV/atom @ 1.5V for all unique formula unit of composition taken from (a) $Mg_xMn_yO_z$ and (b) $Ca_xMn_yO_z$. We plot E^* as function of r defined as ratio of alkaline metal among the non-oxygen elements.

S4. Computed E_{hull} at tier 2

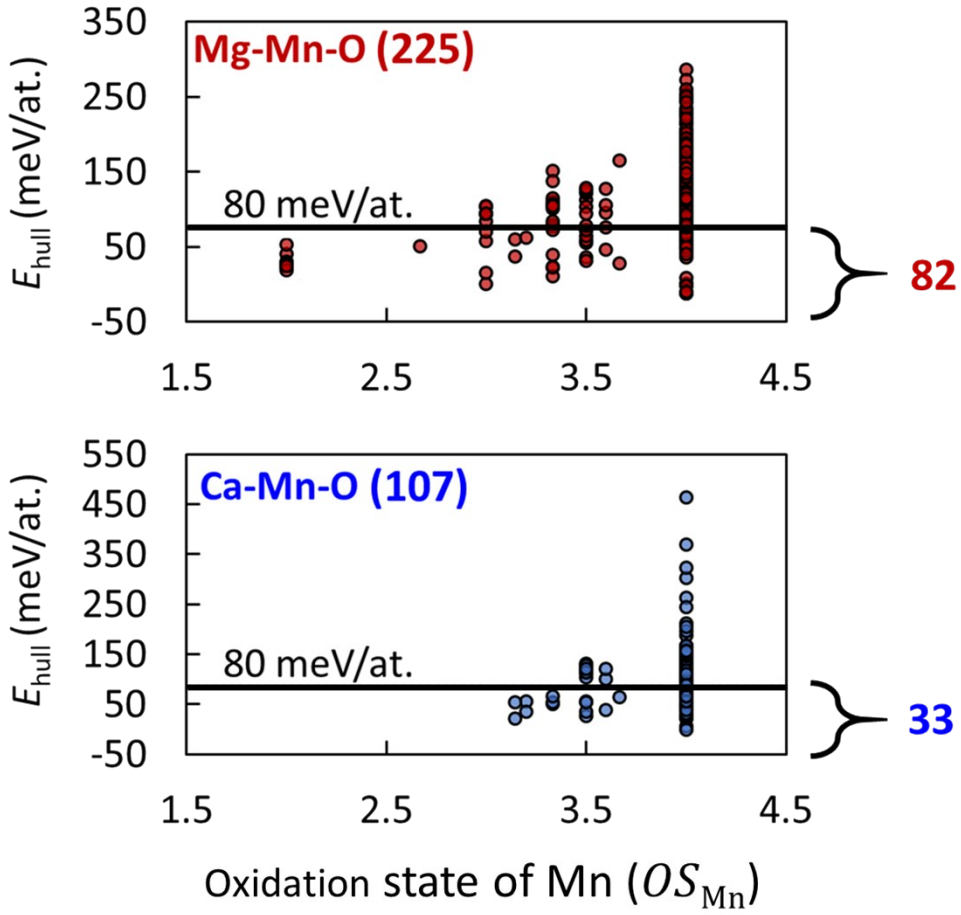

Fig. S6 Computed the energy of the convex hull (E_{hull}) of the 332 materials taken from the tier 1 (a) $Mg_xMn_yO_z$ (225) and (b) $Ca_xMn_yO_z$ (107). We plot E_{hull} as function of oxidation state of Mn (OS_{Mn}) assuming Ca and Mg are +2 and O is -2, and find total 115 meta-stable materials (82 for Mg-Mn-O and 33 for Ca-Mn-O) E_{hull} of which is lower than 80 meV/atom.

S5. Computed materials properties (E_{hull}, ΔG_{pbx}^{min} and E_g^{HSE}) for 82 Mg-Mn-O

Among the listed 82 Mg-Mn-O as shown in Fig. 2 in the main text, bold means materials obtained from tier 3 and red color means materials obtained from tier 4 as shown in Fig. 3 in the main text. We also listed original MP-id used in this work, and element changed to Mg for elemental substitution process.

Original MP-id	Changed to Mg	E_{hull} (eV/atom)	ΔG_{pbx}^{min} (eV/atom)	E_g^{HSE} (eV)
mp-1019541	Ca	0.041	0.65	-
mp-10543	K	0.025	0.62	-
mp-1095270	Na	0.025	0.43	-
mp-15391	Na	0.025	0.51	-
mp-30120	K	0.026	0.62	-
mp-34842	Na	0.028	0.62	-
mp-38489	Co	0.027	0.34	-
mp-4426	Li	0.053	0.56	-
mp-5327	Na	0.027	0.51	-
mp-625768	H	0.03	0.52	-
mp-752910	Na	0.028	0.62	-
mp-760490	Mg	0.027	0.56	-
mp-761360	Cd	0.025	0.29	-
mp-765797	Ni	0.025	0.29	-
mp-765902	Ni	0.026	0.51	-
mp-767029	Mn	0.026	0.34	-
mp-767160	Ca	0.026	0.44	-
mp-767998	Mn	0.019	0.27	-
mp-772385	Co	0.025	0.31	-
mp-754638	Na	0.05	0.66	-
mp-1096958	Dy	0	0.57	-
mp-754843	Na	0.058	0.6	-
mp-778713	Na	0.07	0.62	-
mvc-10002	Ca	0.016	0.6	-
mp-763608	Li	0.06	0.55	-
mp-765454	Ti	0.037	0.5	-
mp-762287	Li	0.062	0.6	-
mp-1003317	H	0.079	0.56	-
mp-18761	K	0.077	0.52	-
mp-19448	Te	0.023	0.42	-
mp-33461	Li	0.011	0.37	-
mp-762236	Cr	0.039	0.46	-

mp-762411	Li	0.073	0.55	-
mp-767090	Fe	0.023	0.39	-
mp-1003312	K	0.055	0.42	-
mp-1003483	Ca	0.037	0.37	-
mp-35530	Li	0.059	0.43	-
mp-752546	Li	0.031	0.35	-
mp-756035	Li	0.065	0.44	-
mp-770104	Li	0.073	0.46	-
mvc-10706	Mg	0.073	0.46	-
mvc-600	Ba	0.079	0.48	-
mp-762390	Li	0.076	0.42	-
mp-773247	Li	0.046	0.39	-
mp-752918	Na	0.027	0.26	-
mp-1006058	U	0.066	0.34	-
mp-1019598	Ce	0.075	0.29	-
mp-1020112	Mg	0.072	0.23	-
mp-1020623	**Si**	**0**	**0.1**	**3.50**
mp-1020631	Ge	0.059	0.25	-
mp-1078830	Se	0.075	0.29	-
mp-18870	**Cd**	**0.001**	**0.13**	**3.02**
mp-19239	**Mg**	**0**	**0.02**	**3.72**
mp-19260	Li	0.065	0.22	-
mp-21137 (Mg_2MnO_4-b)	**Ca**	**0.036**	**0.15**	**2.86**
mp-22747	**C**	**-0.012**	**0.04**	**3.35**
mp-33297 (Mg_2MnO_4-a)	**Mg**	**0.009**	**0.08**	**2.62**
mp-4930	Ti	0.059	0.32	-
mp-4995	Li	0.051	0.23	-
mp-504567 ($Mg_2Mn_3O_8$)	**Cu**	**-0.002**	**0.12**	**2.98**
mp-545482	Pd	0.05	0.23	-
mp-546142	**Na**	**-0.011**	**0.04**	**3.32**
mp-554678	Ca	0.059	0.32	-
mp-555390	Tc	0.076	0.29	-
mp-557997	Se	0.065	0.26	-
mp-560165	Bi	0.064	0.21	-
mp-603907	Mg	0.065	0.27	-
mp-675953	Tl	0.076	0.24	-
mp-763319	V	0.067	0.2	-
mp-763580	Fe	0.079	0.3	-

mp-763580	Li	0.077	0.3	-
mp-765812	Ti	0.045	0.21	-
mp-768065	Cr	0.08	0.3	-
mp-769640	Cr	0.068	0.27	-
mp-769640	V	0.053	0.23	-
mp-769855	Sr	0.054	0.24	-
mp-770778	Cr	0.065	0.27	-
mp-770779	Cr	0.05	0.23	-
mp-771763	Mg	0.04	0.23	-
mp-775827	Cr	0.076	0.29	-
mp-849466	Mn	0.079	0.22	-
mp-8710	**Ca**	**-0.01**	**0.1**	**3.07**

S6. Computed materials properties (E_{hull}, ΔG_{pbx}^{min} and E_g^{HSE}) for 33 Ca-Mn-O

Among the listed 33 Ca-Mn-O as shown in Fig. 2 in the main text, bold means materials obtained from tier 3 and blue color means materials obtained from tier 4 as shown in Fig. 3 in the main text. We listed original MP-id used in this work, and element changed to Ca for elemental substitution process. We note that $Ca_2Mn_3O_8$ materials marked as yellow is the most stable alkaline-based Mn-O material taken from ref [16].

Original MP-id	Changed to Mg	E_{hull} (eV/atom)	ΔG_{pbx}^{min} (eV/atom)	E_g^{HSE} (eV)
mvc-13425 ($Ca_2Mn_3O_8$ [1])	Mg	0.006	0.16	3.00
mp-8710	**Ca**	**0.023**	**0.2**	**2.73**
mp-22955	**I**	**0.022**	**0.29**	**3.26**
mp-7538	La	0.027	0.31	-
mp-762390 ($CaMn_5O_{10}$)	**Li**	**0.039**	**0.34**	**1.89**
mp-754246	Sn	0.04	0.34	-
mp-23487	K	0.045	0.35	-
mp-769855	Sr	0.046	0.35	-
mp-1003483 ($CaMn_4O_8$)	**Ca**	**0.027**	**0.36**	**1.8**
mp-24902	Bi	0.048	0.36	-
mp-568977	Sr	0.049	0.36	-
mp-753948	Pr	0.05	0.36	-
mp-752918 ($CaMn_6O_{12}$)	**Na**	**0.065**	**0.37**	**2.03**
mp-1003312	K	0.036	0.38	-
mp-762225	C	0.062	0.39	-
mp-760461	B	0.069	0.41	-
mp-780619	Rb	0.077	0.43	-
mp-776199	Ag	0.077	0.43	-
mvc-10702	Ca	0.056	0.43	-
mp-762508	Mg	0.08	0.44	-
mp-770352	Eu	0.032	0.45	-
mvc-10923	Fe	0.039	0.46	-
mp-769733	Li	0.021	0.48	-
mp-7982	Mg	0.057	0.51	-
mp-754005	C	0.066	0.53	-
mp-761295	Cd	0	0.53	-
mp-770690	Te	0.051	0.54	-
mp-762411	Li	0.054	0.55	-
mp-753055	Tb	0.056	0.57	-

mp-765454	Ti	0.055	0.57	-
mp-763697	Li	0.067	0.58	-
mp-24955	Sr	0.055	0.6	-
mp-764347	Na	0.036	0.62	-

References

1. J. P. Perdew, K. Burke and M. Ernzerhof, *Physical review letters*, 1996, **77**, 3865.
2. V. I. Anisimov, F. Aryasetiawan and A. Lichtenstein, *Journal of Physics: Condensed Matter*, 1997, **9**, 767.
3. P. E. Blöchl, *Physical Review B*, 1994, **50**, 17953.
4. G. Kresse and J. Furthmüller, *Phys. Rev. B*, 1996, **54**, 169.
5. A. Jain, S. P. Ong, G. Hautier, W. Chen, W. D. Richards, S. Dacek, S. Cholia, D. Gunter, D. Skinner and G. Ceder, *Apl Materials*, 2013, **1**, 011002.
6. S. P. Ong, W. D. Richards, A. Jain, G. Hautier, M. Kocher, S. Cholia, D. Gunter, V. L. Chevrier, K. A. Persson and G. Ceder, *Computational Materials Science*, 2013, **68**, 314-319.
7. A. Jain, G. Hautier, S. P. Ong, C. J. Moore, C. C. Fischer, K. A. Persson and G. Ceder, *Physical Review B*, 2011, **84**.
8. J. Heyd, G. E. Scuseria and M. Ernzerhof, *The Journal of chemical physics*, 2003, **118**, 8207-8215.
9. W. Sun and G. Ceder, *Surface Science*, 2013, **617**, 53-59.
10. A. Shinde, S. K. Suram, Q. Yan, L. Zhou, A. K. Singh, J. Yu, K. A. Persson, J. B. Neaton and J. M. Gregoire, *ACS Energy Letters*, 2017, **2**, 2307-2312.
11. Q. Yan, J. Yu, S. K. Suram, L. Zhou, A. Shinde, P. F. Newhouse, W. Chen, G. Li, K. A. Persson and J. M. Gregoire, *Proceedings of the National Academy of Sciences*, 2017, **114**, 3040-3043.
12. S. K. Suram, L. Zhou, N. Becerra-Stasiewicz, K. Kan, R. J. R. Jones, B. M. Kendrick and J. M. Gregoire, *Rev. Sci. Instrum.*, 2015, **86**, 033904-033904.
13. J. M. Gregoire, D. G. Van Campen, C. E. Miller, R. J. Jones, S. K. Suram and A. Mehta, *Journal of synchrotron radiation*, 2014, **21**, 1262-1268.
14. S. C. Mannsfeld, M. L. Tang and Z. Bao, *Adv. Mater.*, 2011, **23**, 127-131.
15. J. M. Gregoire, C. X. Xiang, X. N. Liu, M. Marcin and J. Jin, *Review of Scientific Instruments*, 2013, **84**.
16. A. K. Singh, L. Zhou, A. Shinde, S. K. Suram, J. H. Montoya, D. Winston, J. M. Gregoire and K. A. Persson, *Chemistry of Materials*, 2017, **29**, 10159-10167.
17. L. Zhou, Q. Yan, J. Yu, R. J. Jones, N. Becerra-Stasiewicz, S. K. Suram, A. Shinde, D. Guevarra, J. B. Neaton and K. A. Persson, *Physical Chemistry Chemical Physics*, 2016, **18**, 9349-9352.